

Captivity-Escape Games as a Means for Safety in Online Motion Generation

Christopher Bohn, Manuel Hess, and Sören Hohmann, *Senior Member, IEEE*

Abstract—This paper presents a method that addresses the conservatism, computational effort, and limited numerical accuracy of existing frameworks and methods that ensure safety in online model-based motion generation, commonly referred to as fast and safe tracking. Computational limitations restrict online motion planning to low-fidelity models. However, planning with low-fidelity models compromises safety, as the dynamic feasibility of resulting reference trajectories is not ensured. This potentially leads to unavoidable tracking errors that may cause safety-critical constraint violations. Existing frameworks mitigate this safety risk by augmenting safety-critical constraints in motion planning by a safety margin that prevents constraint violations under worst-case tracking errors. However, the methods employed in these frameworks determine the safety margin based on a heuristically selected performance of the planning model, which likely results in overly conservative reference trajectories. Furthermore, these methods are computationally intensive, and the state-of-the-art method is limited in numerical accuracy. We adopt a different perspective and address these limitations with a method that mitigates conservatism in existing frameworks by adapting the planning model performance to a given safety margin. Our method achieves numerical accuracy and requires significantly less computation time than existing methods by leveraging a captivity-escape game, which is a specific zero-sum differential game formulated in this paper. We demonstrate our method using a numerical example and compare it to the state of the art.

Index Terms—Differential games, model mismatch, motion generation, safe-by-design, tracking control.

I. INTRODUCTION

Motion generation comprises two tasks: motion planning and tracking of reference trajectories [1], [2], [3], [4]. Both tasks are crucial for the functional safety of an autonomous system [5], and therefore, formally ensuring the safety of motion planning and tracking is essential [1], [2], [3], [4], [6], [7]. Formally ensuring safety requires the accurate consideration of the real-world system dynamics through the use of a high-fidelity model [1], [2], [3], [4].

Definition 1: A high-fidelity model of a dynamic system is given by a state vector $\mathbf{x}_h(t) \in \mathcal{X}_h \subseteq \mathbb{R}^n$, $\mathbf{x}_h : \mathbb{R} \rightarrow \mathcal{X}_h$, an input vector $\mathbf{u}_h(t) \in \mathcal{U}_h \subseteq \mathbb{R}^{q_h}$, $\mathbf{u}_h : \mathbb{R} \rightarrow \mathcal{U}_h$, a parameter vector $\boldsymbol{\iota}_h \in \mathbb{R}^{z_h}$, and an ordinary differential equation (ODE)

$$\dot{\mathbf{x}}_h(t) = \mathbf{f}_h^{\iota_h}(\mathbf{x}_h(t), \mathbf{u}_h(t)). \quad (1)$$

The authors are with the Institute of Control Systems, Karlsruhe Institute of Technology, 76131 Karlsruhe, Germany. Corresponding author is Christopher Bohn (e-mail: christopher.bohn@kit.edu).

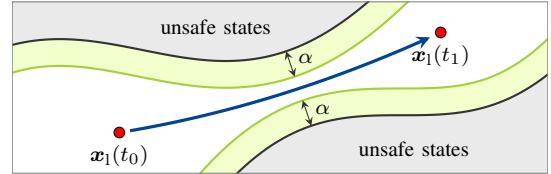


Fig. 1 The figure illustrates the task of planning a reference trajectory from $\mathbf{x}_1(t_0)$ to $\mathbf{x}_1(t_1)$, indicated by the blue arrow. The gray regions indicate unsafe states (e.g., obstacles), the black lines indicate safety-critical constraints, and the green regions indicate the safety margin α .

The set \mathcal{U}_h is compact, $\mathbf{f}_h^{\iota_h} : \mathcal{X}_h \times \mathcal{U}_h \rightarrow \mathcal{X}_h$ is Lipschitz continuous in $\mathbf{x}_h(t)$ for a fixed $\mathbf{u}_h(t)$, and continuously differentiable in $\mathbf{x}_h(t)$. Thus, given any measurable function \mathbf{u}_h (see [8]), a unique trajectory exists that solves (1) [9].

Assumption 1: A high-fidelity model of a dynamic system accurately represents the related real-world system dynamics.

Advanced model-based control design methods facilitate the use of a high-fidelity model [1], [2], [3], [4], [10]. Therefore, consider a high-fidelity model to be used for tracking.

Conversely, motion planning requires a substantial prediction horizon and fast computation times, rendering the use of a high-fidelity model impractical due to computational limitations. Consequently, motion planning commonly uses a low-fidelity model [1], [2], [3], [4].

Definition 2: A low-fidelity model of a dynamic system is given by a state vector $\mathbf{x}_l(t) \in \mathcal{X}_l \subseteq \mathcal{X}_h$, $\mathbf{x}_l : \mathbb{R} \rightarrow \mathcal{X}_l$, with $\dim \mathcal{X}_l = m$, an input vector $\mathbf{u}_l(t) \in \mathcal{U}_l \subseteq \mathbb{R}^{q_l}$, $\mathbf{u}_l : \mathbb{R} \rightarrow \mathcal{U}_l$, a parameter vector $\boldsymbol{\iota}_l \in \mathbb{R}^{z_l}$, and an ODE

$$\dot{\mathbf{x}}_l(t) = \mathbf{f}_l^{\iota_l}(\mathbf{x}_l(t), \mathbf{u}_l(t)). \quad (2)$$

The properties of the set \mathcal{U}_l and the function $\mathbf{f}_l^{\iota_l}$ match those of \mathcal{U}_h and $\mathbf{f}_h^{\iota_h}$, respectively.

Crucially, reference trajectories planned with a low-fidelity model are not necessarily dynamically feasible for the high-fidelity tracking model. This potentially results in unavoidable tracking errors that may cause violations of safety-critical constraints, thus posing a safety risk in motion generation.

To address this safety risk, the frameworks in [1], [2], [3], [4] augment safety-critical constraints in motion planning by a safety margin $\alpha \in \mathbb{R}^+$ that ensures preventing constraint violations under the worst-case tracking error (WTE) (see Fig. 1). In addition, a safety controller is used to ensure the tracking error does not exceed α . The methods employed in these frameworks determine both the safety margin α and controller based on a specific pair of low-fidelity and high-fidelity models. Note that \mathcal{X}_h , \mathcal{U}_h , and $\boldsymbol{\iota}_h$ can be determined via

system identification, whereas \mathcal{X}_1 , \mathcal{U}_1 , and \mathbf{u}_1 must be selected heuristically to suit the planning task. We denote the objective of determining α for a specific pair of models as O.0.

Objective O.0: Compute a safety margin α that ensures safe motion generation with given $\mathbf{f}_1^{\ell_1}$, \mathcal{X}_1 , \mathcal{U}_1 , \mathbf{u}_1 , $\mathbf{f}_h^{\ell_h}$, \mathcal{X}_h , \mathcal{U}_h , \mathbf{u}_h .

However, addressing O.0 with the methods in [1], [2], [3] is computationally intensive, and the numerical accuracy of the safety margin α resulting from [1], [2] is not ensured [4]. Moreover, the heuristically selected \mathcal{X}_1 , \mathcal{U}_1 , and \mathbf{u}_1 , and the resulting safety margin α are likely ill-suited to a given planning task, leading to overly conservative reference trajectories.¹

To mitigate the existing framework's conservatism, \mathcal{X}_1 , \mathcal{U}_1 , and \mathbf{u}_1 must be adapted to a safety margin α that suits the specific planning task. However, adapting \mathcal{X}_1 , \mathcal{U}_1 , \mathbf{u}_1 to a given α using the methods in [1], [2], [3] entails iteratively tuning \mathcal{X}_1 , \mathcal{U}_1 , \mathbf{u}_1 and recomputing α , which is computationally intractable.

In this paper, we address these limitations by presenting a computationally efficient and numerically accurate method that adapts \mathcal{X}_1 , \mathcal{U}_1 , and \mathbf{u}_1 to a given safety margin α , thereby focusing on the following objectives:

Objective O.1: Directly compute \mathcal{X}_1 , \mathcal{U}_1 , and \mathbf{u}_1 that ensure safe motion generation with given α , $\mathbf{f}_1^{\ell_1}$, $\mathbf{f}_h^{\ell_h}$, \mathcal{X}_h , \mathcal{U}_h , and \mathbf{u}_h .

Objective O.2: Design a safety controller that ensures safe tracking within a given safety margin α , given $\mathbf{f}_h^{\ell_h}$, \mathcal{X}_h , \mathcal{U}_h , \mathbf{u}_h , and $\mathbf{f}_1^{\ell_1}$, with \mathcal{X}_1 , \mathcal{U}_1 , and \mathbf{u}_1 as determined per O.1.

A. Related Work

In [1], [2], the authors present the state-of-the-art method for addressing O.0 and the state-of-the-art framework that uses a safety margin to ensure safe motion generation, named fast and safe tracking (FaSTrack). The method presented in [1], [2] uses a pursuit-evasion differential game to determine a safety margin and the associated safety controller. The related computations are intensive, as the utilized pursuit-evasion game must be solved numerically using Hamilton-Jacobi reachability analysis [8].² Moreover, the numerical accuracy of the resulting safety margin cannot be ensured because of the numerical methods involved [4]. This poses a safety risk in FaSTrack. Furthermore, the FaSTrack framework uses a fixed safety margin and fixed \mathcal{X}_1 , \mathcal{U}_1 , and \mathbf{u}_1 for various planning environments, which likely causes planning overly conservative reference trajectories [11].

In [11], the authors build upon FaSTrack and reduce conservatism by using a set of motion planners that feature different safety margins. A meta-planning algorithm is used to online select a planner that suits the planning environment. However, [11] remains conservative, as the set of available planners is limited due to FaSTrack's computational intensity. In addition, [11] inherits FaSTrack's limited numerical accuracy.

In [12], a method is presented that builds upon FaSTrack and reduces conservatism by constraining motion planning to

¹Nonrestrictive \mathcal{X}_1 , \mathcal{U}_1 , and \mathbf{u}_1 enable dynamic reference trajectories but result in a large WTE, thus requiring a large safety margin α . A large α shrinks the planning space and potentially renders the planning task infeasible (e.g., if the safety margin α in Fig. 1 was larger, it would close the gap between $\mathbf{x}_1(t_0)$ to $\mathbf{x}_1(t_1)$). Conversely, restrictive \mathcal{X}_1 , \mathcal{U}_1 , and \mathbf{u}_1 only require a small safety margin α but result in low-performance trajectories.

²Determining a safety margin with decent accuracy takes days, even if both the planning model and the tracking model are simple and low-dimensional.

motion primitives. However, this restricts resulting reference trajectories to compositions of a limited set of primitives.

The authors in [3] present a method to address O.0 by computing a safety margin and a safety controller using sum-of-squares optimization. However, compared to FaSTrack, the method in [3] results in a more conservative safety margin.

In [4], a motion generation framework that ensures safety by utilizing a safety margin is presented. However, addressing O.0 is not the focus of [4].

The objective O.1 remains unaddressed in the literature. All related works focus on O.0, necessitating heuristic selection of \mathcal{X}_1 , \mathcal{U}_1 , and \mathbf{u}_1 . In addition, all existing methods are computationally intensive, and the methods based on the state of the art (FaSTrack) do not ensure numerical accuracy.

B. Contribution

The contribution of this work is a method that addresses O.1, O.2, and, as it turns out, even O.0. The presented method is based on a captivity-escape game, which is a specific zero-sum differential game with two players. The results determined with the presented method are numerically accurate³ and the computation time of the presented method is significantly faster⁴ than the computation time of the state-of-the-art method FaSTrack. Consequently, our method complements the frameworks presented in [1], [2], [3], [4] by reducing computation time, ensuring accuracy, and mitigating conservatism. We demonstrate the presented method using a numerical example and compare it to the state-of-the-art method FaSTrack.

C. Outline

In Section II, we formulate the problems related to O.1 and O.2. In Section III, we introduce captivity-escape differential games, which we leverage in Section IV to address the problems related to O.1 and O.2. Solving captivity-escape games is addressed in Section V, and a numerical example in Section VI demonstrates the presented method.

II. PROBLEM FORMULATION

In this section, we formulate the problems related to addressing O.1 and O.2. To this end, we formulate the relative system between a high-fidelity model and a low-fidelity model and define the WTE along with associated quantities.

A. Formulation of the Relative System

Definition 3: The tracking error between a high-fidelity tracking model (see Definition 1) and a low-fidelity planning model (see Definition 2) is given by the so-called relative state vector $\mathbf{x}(t) \in \mathcal{X} \subseteq \mathbb{R}^n$, $\mathbf{x} : \mathbb{R} \rightarrow \mathcal{X}$ with

$$\mathbf{x}(t) := \Phi(\mathbf{x}_1(t), \mathbf{x}_h(t)) (Q\mathbf{x}_1(t) - \mathbf{x}_h(t)). \quad (3)$$

³Depending on the employed models, computations are either performed analytically or utilize numerical integration. Approaches exist for determining the errors resulting from numerical integration to ensure safety [13, Chap. 9].

⁴We consider the computation time of the presented method to be within the timescale that allows for online adaption of \mathcal{X}_1 , \mathcal{U}_1 , and \mathbf{u}_1 .

The matrix Q is a projection matrix from \mathcal{X}_l to \mathcal{X}_h , and $\Phi(x_l(t), x_h(t))$ is a Lipschitz continuous map that must be determined such that the relative system dynamics

$$\dot{x}(t) = f^\iota(x(t), u_l(t), u_h(t)) \quad (4)$$

are given by a function $f^\iota : \mathcal{X} \times \mathcal{U}_l \times \mathcal{U}_h \rightarrow \mathcal{X}$ that is Lipschitz continuous in $x(t)$ for fixed $u_l(t)$ and $u_h(t)$, and continuously differentiable in $x(t)$, with $\iota = [\iota_l \ \iota_h] \in \mathbb{R}^{z_l + z_h}$.⁵

Thus, given an initial state $x(t_0)$ and any measurable input functions u_l and u_h , a unique solution trajectory of (4) exists

$$\xi(t; t_0, x(t_0), u_l, u_h) : [t_0, t] \rightarrow \mathcal{X}, \quad (5)$$

which satisfies $\xi(t_0; t_0, x(t_0), u_l, u_h) = x(t_0)$ and

$$\begin{aligned} \dot{\xi}(t; t_0, x(t_0), u_l, u_h) = \\ f^\iota(\xi(t; t_0, x(t_0), u_l, u_h), u_l(t), u_h(t)) \end{aligned} \quad (6)$$

almost everywhere [8], [14].

B. Problems Related to Addressing O.1 and O.2

As addressing O.1 relates to determining the sets \mathcal{X}_l , \mathcal{U}_l , and the vector ι_l , we assume that \mathcal{X}_l , \mathcal{U}_l , and ι_l can be determined by means of a single parameter.

Assumption 2: The sets \mathcal{X}_l and \mathcal{U}_l can be parametrized such that each set is fully defined by a vector $\chi_{\mathcal{X}_l}$ and $\chi_{\mathcal{U}_l}$, respectively, containing the related parameters.

Definition 4: Let Assumption 2 be fulfilled. The vector $\theta \in \mathbb{R}^s$ with $\theta = [\chi_{\mathcal{X}_l} \ \chi_{\mathcal{U}_l} \ \iota_l]$ fully defines \mathcal{X}_l , \mathcal{U}_l , and ι_l .

Definition 5: The mapping $\mathbf{o}(\vartheta) = \theta$, $\mathbf{o} : \mathbb{R}^+ \rightarrow \mathbb{R}^s$ determines \mathcal{X}_l , \mathcal{U}_l , and ι_l by means of the so-called planning performance $\vartheta \in \mathbb{R}^+$.

Assumption 3: The mapping $\mathbf{o}(\vartheta) = \theta$ is given such that a larger ϑ results in a better performance of the planning model.

In addition, addressing O.1 and O.2 requires a formal relation between ϑ , a safety margin α , and a safety controller.

Definition 6: The mapping $u_h = \varsigma_h(x)$, with $\varsigma_h : (\mathbb{R} \rightarrow \mathcal{X}) \rightarrow (\mathbb{R} \rightarrow \mathcal{U}_h)$ denotes a state-feedback strategy.

Definition 7: The mapping $u_l = \gamma_l(x, u_h)$, with $\gamma_l : (\mathbb{R} \rightarrow \mathcal{X}) \times (\mathbb{R} \rightarrow \mathcal{U}_h) \rightarrow (\mathbb{R} \rightarrow \mathcal{U}_l)$ denotes a nonanticipative strategy as formulated in [8].

For brevity, we use the notations $\varsigma_h(x)$ and $\gamma_l(x, u_h)$ to refer to a strategy, and the notations $\varsigma_h(x(t))$ and $\gamma_l(x(t), u_h(t))$ to refer to an input vector resulting from a strategy.

Definition 8: The critical relative state vector $c(x(t)) \in \mathcal{X}$ captures relative states for which safety-critical constraints exist. It is given by the linear mapping $c(x(t)) = P x(t)$, $c : \mathcal{X} \rightarrow \mathcal{X}$, with $P = \text{diag}(p_j)$, $j = 1 \dots n$, and $p_j = 1$, if safety-critical constraints exist for x_j , and $p_j = 0$, otherwise.

Definition 9: A tracking error bound (TEB) is a set $\mathcal{B} \subseteq \mathcal{X}$ with a nonempty and compact $c(\mathcal{B}) \subseteq \mathcal{X}$, and for which a state-feedback strategy $u_h = \varsigma_h(x)$ exists such that for any nonanticipative strategy $u_l = \gamma_l(x, u_h)$ and any initial $x(t_0) \in \mathcal{B} \Rightarrow \forall t \geq t_0 : \xi(t; t_0, x(t_0), \gamma_l(x, u_h), \varsigma_h(x)) \in \mathcal{B}$.

The boundary of \mathcal{B} is denoted as $\partial\mathcal{B}$.

Definition 10: The WTE ζ is $\zeta := \max_{x(t) \in \mathcal{B}} \|c(x(t))\|_2$.

⁵If mobile robots are considered, the map $\Phi(x_l(t), x_h(t))$ is often given by the identity map or a rotation map for various combinations of high-fidelity and low-fidelity models. A discussion on $\Phi(x_l(t), x_h(t))$ is given in [3].

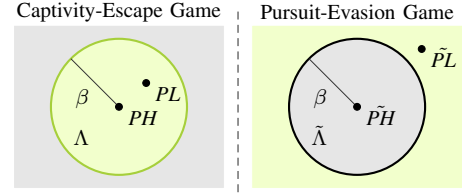


Fig. 2 A valid initial state $x(t_0)$ for both games is depicted by the position of PL (respectively, \tilde{PL}). Each game terminates when PL (respectively, \tilde{PL}) exits the green region into the gray region.

Remark 1: To prevent safety-critical constraint violations under the WTE ζ , a safety margin α must fulfill $\zeta \leq \alpha$.

With Remark 1, a TEB \mathcal{B} and the related WTE ζ establish the required formal relation between the planning performance ϑ (i.e., \mathcal{X}_l , \mathcal{U}_l , and ι_l , see Definition 5), a safety margin α , and a safety controller. To minimize conservatism, the TEB \mathcal{B} must be constituted by means of the state-feedback strategy that is optimal w.r.t. retaining solution trajectories of (4) in \mathcal{B} . This strategy is denoted as $u_h = \varsigma_h^\bullet(x)$. Moreover, the strategy that is optimal w.r.t. forcing solution trajectories of (4) to leave the TEB \mathcal{B} , denoted as $u_l = \gamma_l^\bullet(x, u_h)$, must be used to ensure the TEB \mathcal{B} holds for any $u_l = \gamma_l(x, u_h)$.

Problem 1: Determine the optimal strategies $u_h = \varsigma_h^\bullet(x)$ and $u_l = \gamma_l^\bullet(x, u_h)$ for constituting a TEB \mathcal{B} .

To maintain focus on minimizing conservatism, the planning performance ϑ must be adapted such that the safety margin α is fully utilized by the related WTE ζ , requiring $\zeta = \alpha$.

Problem 2: Determine the planning performance ϑ so that the TEB constituted by means of $u_h = \varsigma_h^\bullet(x)$ and $u_l = \gamma_l^\bullet(x, u_h)$ results in a WTE ζ that fulfills $\zeta = \alpha$.

III. CAPTIVITY-ESCAPE DIFFERENTIAL GAME

In this section, we formulate a specific differential game that is tailored to efficiently address Problem 1 and Problem 2.

A. Formulation of a Captivity-Escape Game

A captivity-escape game is a deterministic zero-sum differential game with variable terminal time T . In the game, there are two players that we refer to as PL and PH . PL employs the dynamics of the low-fidelity planning model (see Definition 2) and is restricted to a nonanticipative strategy $u_l = \gamma_l(x, u_h)$ (see Definition 7). PH employs the dynamics of the high-fidelity tracking model (see Definition 1) and is restricted to a state-feedback strategy $u_h = \varsigma_h(x)$ (see Definition 6). The relative state vector between PL and PH is given by (3), and the relative system dynamics between PL and PH are given by (4). The initial state of the game is denoted as $x(t_0)$.

Definition 11: The so-called captivity set $\Lambda \subseteq \mathcal{X}$ is given by $\Lambda := \{x(t) \in \mathcal{X} \mid \|c(x(t))\|_2 \leq \beta\}$, with $\beta \in \mathbb{R}^+$.

The boundary of the captivity set Λ is denoted as $\partial\Lambda$.

Remark 2: $\forall x(t) \in \partial\Lambda : \|c(x(t))\|_2 = \beta$.

Assumption 4: The game's initial state fulfills $x(t_0) \in \Lambda$.

Definition 12: The objective function J in a captivity-escape game is given by the terminal time T of the game: $J = T := \inf \{t \mid x(t) \notin \Lambda\}$. PL aims to minimize J whereas PH aims to maximize J .

So, PL initializes in *captivity*. In the game, PL seeks to *escape* from Λ by achieving any $\mathbf{x}(t) \notin \Lambda$. Conversely, PH strives to retain PL in Λ by maintaining $\mathbf{x}(t) \in \Lambda$. The game terminates when $\mathbf{x}(t) \notin \Lambda$, marking the escape of PL .

Remark 3: Note the difference between a captivity-escape game and a pursuit-evasion game as employed in [1], [2]. In a pursuit-evasion game, a player \tilde{PL} is initially *free*, and the game terminates when a second player \tilde{PH} captures \tilde{PL} inside a closed target set $\tilde{\Lambda}$ [15]. In contrast, in the formulated captivity-escape game, PL is initially in *captivity*, and the game terminates when PL escapes from the compact captivity set Λ . This shift in perspective, highlighted in Fig. 2, is central for efficiently addressing O.0, O.1, and O.2.

B. Formulation of a Captivity-Escape Game of Kind

For solving Problem 1 and Problem 2, it is sufficient to investigate under what conditions PL can terminate a captivity-escape game by escape, or equivalently, under what conditions the game does not terminate. To this end, consider a captivity-escape game of kind with only two possible outcomes:

- (o.i) Player PH is able to retain eternal captivity despite PL 's best effort to terminate the game by escaping.
- (o.ii) Player PL is able to escape in finite time despite PH 's best effort to retain PL in captivity.

Definition 13: The objective function J_k in a captivity-escape game of kind is given by

$$J_k := \begin{cases} -1 & \text{if } \mathbf{x}(t) \in \Lambda, \forall t \in [t_0, \infty), \\ +1 & \text{otherwise.} \end{cases} \quad (7)$$

Definition 14: In a captivity-escape game of kind, PL aims to maximize J_k whereas PH aims to minimize J_k .

Definition 15: If both players act optimally, the value function $V(\mathbf{x}(t))$ in a captivity-escape game of kind is given by

$$V(\mathbf{x}(t)) = \begin{cases} -1 & \text{if } \mathbf{x}(t_0) \text{ results in (o.i),} \\ +1 & \text{if } \mathbf{x}(t_0) \text{ results in (o.ii).} \end{cases} \quad (8)$$

Definition 16: The set $\mathcal{V}^- \subseteq \Lambda$, with $\mathcal{V}^- := \{\mathbf{x}(t) \in \Lambda \mid V(\mathbf{x}(t)) = -1\}$ forms the so-called captivity zone of Λ .

Definition 17: The set $\mathcal{V}^+ \subseteq \Lambda$, with $\mathcal{V}^+ := \{\mathbf{x}(t) \in \Lambda \mid V(\mathbf{x}(t)) = +1\}$ forms the so-called escape zone of Λ .

Assumption 5: The captivity zone \mathcal{V}^- (see Definition 16) of a captivity-escape game of kind is nonempty and compact. The boundary of \mathcal{V}^- is denoted as $\partial\mathcal{V}^-$.

Definition 18: In a captivity-escape game of kind, the optimal strategies of PL and PH are denoted as $\mathbf{u}_l = \gamma_l^*(\mathbf{x}, \mathbf{u}_h)$ and $\mathbf{u}_h = \varsigma_h^*(\mathbf{x})$, respectively. These optimal strategies are only defined for $\mathbf{x}(t) \in \partial\Lambda$ and $\mathbf{x}(t) \in \partial\mathcal{V}^-$.

Consequently, if both players use their optimal strategy (see Definition 18), trajectories starting in the captivity zone \mathcal{V}^- stay in the captivity set Λ : $\forall \mathbf{x}(t_0) \in \mathcal{V}^- \Rightarrow \forall t \geq t_0$: $\xi(t; t_0, \mathbf{x}(t_0), \gamma_l^*(\mathbf{x}, \mathbf{u}_h), \varsigma_h^*(\mathbf{x})) \in \Lambda$. Thus, we say initializing the game in $\mathbf{x}(t_0) \in \mathcal{V}^-$ results in eternal captivity.

IV. FROM A CAPTIVITY-ESCAPE GAME OF KIND TO A TEB, THE RELATED WTE, AND A SAFETY CONTROLLER

In this section, we formulate the relation between a TEB \mathcal{B} , a WTE ζ , a safety controller, and a captivity-escape game of kind as formulated in Section III-B.

A. Captivity-Escape Game and a TEB

Proposition 1: Consider a trajectory ξ that solves (4) with $\tilde{\mathbf{x}} = \xi(\tilde{t}; t_0, \mathbf{x}(t_0), \gamma_l(\mathbf{x}, \mathbf{u}_h), \varsigma_h(\mathbf{x}))$, $\tilde{t} \geq t_0$. For all $t \geq \tilde{t}$, the trajectory ξ is identical to a second trajectory $\tilde{\xi}$ that solves (4) and starts in $\tilde{\mathbf{x}}$ at \tilde{t} : $\tilde{\xi}(\tilde{t}; t_0, \mathbf{x}(t_0), \gamma_l(\mathbf{x}, \mathbf{u}_h), \varsigma_h(\mathbf{x})) = \xi(\tilde{t}; \tilde{t}, \xi(\tilde{t}; t_0, \mathbf{x}(t_0), \gamma_l(\mathbf{x}, \mathbf{u}_h), \varsigma_h(\mathbf{x})), \gamma_l(\mathbf{x}, \mathbf{u}_h), \varsigma_h(\mathbf{x}))$.

Proof: Follows from the uniqueness of trajectories that solve (4) (see Definition 3). ■

Theorem 1: Let Assumption 5 be fulfilled. The captivity zone \mathcal{V}^- (see Definition 16) forms a TEB \mathcal{B} (see Definition 9) constituted by means of $\mathbf{u}_h = \varsigma_h^*(\mathbf{x})$ (see Definition 18).

Proof: In a captivity-escape game of kind, trajectories that solve (4) and start in \mathcal{V}^- stay in Λ (see Definition 16). For remaining in Λ , these trajectories must also remain in \mathcal{V}^- , for if they did not, $\tilde{\mathbf{x}} = \xi(\tilde{t}; t_0, \mathbf{x}(t_0), \gamma_l^*(\mathbf{x}, \mathbf{u}_h), \varsigma_h^*(\mathbf{x}))$ with $\tilde{t} > t_0$, $\mathbf{x}(t_0) \in \mathcal{V}^-$, and $\tilde{\mathbf{x}} \in \mathcal{V}^+$ would imply $\xi(\tilde{t}; t_0, \mathbf{x}(t_0), \gamma_l^*(\mathbf{x}, \mathbf{u}_h), \varsigma_h^*(\mathbf{x})) = \tilde{\xi}(\tilde{t}; \tilde{t}, \xi(\tilde{t}; t_0, \mathbf{x}(t_0), \gamma_l^*(\mathbf{x}, \mathbf{u}_h), \varsigma_h^*(\mathbf{x})), \gamma_l^*(\mathbf{x}, \mathbf{u}_h), \varsigma_h^*(\mathbf{x}))$, $\forall t \geq \tilde{t}$ (see Proposition 1), which contradicts Definition 16. ■

B. Captivity-Escape Game and a WTE

Theorem 2: Let Assumption 5 be fulfilled. The size β of the captivity set Λ (see Definition 11) is an upper bound of the WTE ζ (see Definition 10) related to the TEB \mathcal{B} (see Definition 9) formed by \mathcal{V}^- (see Theorem 1): $\zeta \leq \beta$.

Proof: The largest possible WTE $\hat{\zeta}$ corresponds to the largest possible TEB $\hat{\mathcal{B}}$ (see Definition 10) which is given by the largest possible $\hat{\mathcal{V}}^-$ (see Theorem 1). As $\mathcal{V}^- \subseteq \Lambda$ (see Definition 16), $\hat{\mathcal{B}} = \Lambda$, and thus, $\hat{\zeta} = \max_{\mathbf{x}(t) \in \hat{\mathcal{B}}} \|\mathbf{c}(\mathbf{x}(t))\|_2 = \max_{\mathbf{x}(t) \in \Lambda} \|\mathbf{c}(\mathbf{x}(t))\|_2 = \beta$ (see Definition 10, Remark 2). ■

Corollary 1: The size β of the captivity set Λ serves as a safety margin α : $\zeta \leq \beta = \alpha$ (see Remark 1).

Assumption 6: The captivity zone \mathcal{V}^- contains at least one state on the boundary of the captivity set $\partial\Lambda$: $\mathcal{V}^- \cap \partial\Lambda \neq \emptyset$.

Corollary 2: Let Assumption 5 and Assumption 6 be fulfilled: $\zeta = \beta = \alpha$ holds (see Theorem 2 and Corollary 1).

Corollary 2 indicates that under Assumption 5 and Assumption 6, a captivity-escape game of kind can be used to solve Problem 2 with $\zeta = \alpha$.

C. Captivity-Escape Game and a Safety Controller

Theorem 3: Let Assumption 5 be fulfilled. The strategy

$$\bar{\varsigma}(\mathbf{x}) := \begin{cases} \varsigma_h^*(\mathbf{x}) & \text{if } \mathbf{x}(t) \in \partial\mathcal{B}, \\ \text{any } \mathbf{u}_h & \text{if } \mathbf{x}(t) \in \text{int}(\mathcal{B}), \end{cases} \quad (9)$$

ensures that for any $\mathbf{x}(t_0) \in \mathcal{B}$ and any $\mathbf{u}_l = \gamma_l(\mathbf{x}, \mathbf{u}_h)$: $\xi(\tilde{t}; t_0, \mathbf{x}(t_0), \gamma_l(\mathbf{x}, \mathbf{u}_h), \bar{\varsigma}(\mathbf{x})) \in \mathcal{B}$ holds $\forall t \geq t_0$.

Proof: To leave \mathcal{B} , $\xi(\tilde{t}; t_0, \mathbf{x}(t_0), \gamma_l(\mathbf{x}, \mathbf{u}_h), \bar{\varsigma}(\mathbf{x}))$ with $\mathbf{x}(t_0) \in \mathcal{B}$ must pass a state $\mathbf{x}(t) \in \partial\mathcal{B}$. Thus, it is sufficient to show that $\bar{\varsigma}(\mathbf{x})$ ensures for any $\mathbf{x}(t_0) \in \partial\mathcal{B}$ and any $\mathbf{u}_l = \gamma_l(\mathbf{x}, \mathbf{u}_h)$: $\xi(\tilde{t}; t_0, \mathbf{x}(t_0), \gamma_l(\mathbf{x}, \mathbf{u}_h), \bar{\varsigma}(\mathbf{x})) \in \mathcal{B}$ holds $\forall t \geq t_0$ (see Proposition 1). This follows from Definition 18 and Theorem 1, as any $\gamma_l(\mathbf{x}, \mathbf{u}_h)$ is equally optimal or suboptimal compared to $\gamma_l^*(\mathbf{x}, \mathbf{u}_h)$. ■

Corollary 3: The strategy $\mathbf{u}_h = \bar{\varsigma}(\mathbf{x})$ serves as a minimal-intervention safety controller under which the TEB \mathcal{B} is positively invariant.

Corollary 4: The strategies $\gamma_1^\bullet(x, u_h)$ and $\varsigma_h^\bullet(x)$ in Problem 1 are given by $\gamma_1^*(x, u_h)$ and $\varsigma_h^*(x)$, for $x(t) \in \partial\mathcal{B}$.

V. SOLVING A CAPTIVITY-ESCAPE GAME OF KIND FOR ADDRESSING O.0, O.1 AND O.2

In this section, we present a method for solving a captivity-escape game of kind to determine the captivity zone \mathcal{V}^- that constitutes a TEB \mathcal{B} (see Theorem 1). To this end, we outline an existing method for solving games of kind in Section V-A and complement this method in Section V-B to address the objectives presented in Section I.

A. Solving a Captivity-Escape Game of Kind with a Given Planning Performance and Safety Bound

In this section, we outline the method in [16, Chap. 8], tailored to determining the captivity zone \mathcal{V}^- in a captivity-escape game of kind. Within this section, assume a suitable planning performance ϑ and safety margin α to be given, ensuring the game can be solved with the outlined method. The principle of this method lies in determining the captivity zone \mathcal{V}^- by constructing $\partial\mathcal{V}^-$ using the so-called nonusable part (NUP) of $\partial\Lambda$ and a so-called closed barrier surface \mathcal{K} that subdivides Λ into \mathcal{V}^- and \mathcal{V}^+ .

1) The Nonusable Part of $\partial\Lambda$:

Definition 19: The vector $\eta_x \in \mathbb{R}^n$ denotes the outward normal to the captivity set Λ at a state $x(t) \in \partial\Lambda$.

Player *PL* cannot terminate the game instantaneously by escaping from a state $x(t) \in \partial\Lambda$ where

$$\min_{u_h(t) \in \mathcal{U}_h} \max_{u_1(t) \in \mathcal{U}_1} \eta_x^\top f^t(x(t), u_1(t), u_h(t)) \leq 0, \quad (10)$$

if *PH* behaves optimally [16, Sec. 4.7]. The order of the min and max operator in (10) is fixed, as *PH* uses a state-feedback strategy and *PL* uses a nonanticipative strategy (see [8]).

Definition 20 ([16, Sec. 4.7]): The states $x(t) \in \partial\Lambda$ satisfying (10) constitute the so-called NUP of $\partial\Lambda$.

Definition 21 ([16, Sec. 4.7]): The states $x(t) \in \partial\Lambda$ satisfying equality in (10) constitute the so-called boundary of the nonusable part (BNUP) that is denoted as $\mathcal{S} \subseteq \partial\Lambda$.

Remark 4: By solving (10) for equality, the BNUP \mathcal{S} can be determined as a mapping $\mathbf{a}(\kappa)$, $\mathbf{a} : \mathbb{R}^r \rightarrow \mathcal{S}$. The vector $\kappa \in \mathbb{R}^r$ relates to the states for which no safety-critical constraints exist (see Definition 8).

Consider the optimal strategies w.r.t. (10) to be denoted as $u_h = \varsigma_h^\Delta(x)$ and $u_1 = \gamma_1^\Delta(x, u_h)$. Definition 20 indicates that a solution trajectory of (4) $\xi(t; t_0, x(t_0), \gamma_1(x, u_h), \varsigma_h^\Delta(x))$ cannot cross the NUP for any $u_1 = \gamma_1(x, u_h)$. Thus, the NUP qualifies for constructing a part of $\partial\mathcal{V}^-$.

2) The Closed Barrier that Subdivides Λ into \mathcal{V}^- and \mathcal{V}^+ :

The surface that separates \mathcal{V}^- from \mathcal{V}^+ must not be crossed in optimal play. Thus, it must be semipermeable [16, Sec. 8.5].

Definition 22: The nonzero vector $\psi_x \in \mathbb{R}^n$ denotes an outward normal to a smooth surface $\mathcal{L} \subseteq \mathbb{R}^n$ at $x(t) \in \mathcal{L}$.

Definition 23 ([16, Sec. 8.3]): A surface \mathcal{L} is semipermeable, if for all $x(t) \in \mathcal{L}$

$$\min_{u_h(t) \in \mathcal{U}_h} \max_{u_1(t) \in \mathcal{U}_1} \psi_x^\top f^t(x(t), u_1(t), u_h(t)) = 0. \quad (11)$$

Definition 24 ([17, Sec. 5.3]): One or more semipermeable surfaces \mathcal{L} that jointly separate \mathcal{V}^- from \mathcal{V}^+ constitute a so-called closed barrier $\mathcal{K} \subseteq \mathcal{V}^-$.

Note that $\mathcal{K} \subseteq \mathcal{V}^-$ (see Definition 24) means that the game does not terminate for initialization in $x(t_0) \in \mathcal{K}$, if both players act optimally. This aligns with the formulation of a captivity-escape game given in Section III but differs from [16], where a distinct game is considered.

3) Determining the Captivity Zone \mathcal{V}^- by Means of $\partial\mathcal{V}^-$:

The boundary of the captivity zone $\partial\mathcal{V}^-$ is constructed by determining semipermeable surfaces \mathcal{L} that jointly constitute a closed barrier \mathcal{K} that smoothly connects to the NUP at the BNUP [16, Sec. 8.5]. Note that by designing \mathcal{K} such that it connects to the BNUP, Assumption 6 is automatically fulfilled.

Consider the optimal strategies w.r.t. (11) to be denoted as $u_1 = \gamma_1^\diamond(x, u_h)$ and $u_h = \varsigma_h^\diamond(x)$. Substituting $\gamma_1^\diamond(x, u_h)$ and $\varsigma_h^\diamond(x)$ into (11) yields the identity

$$\psi_x^\top f^t(x(t), \gamma_1^\diamond(x(t), \varsigma_h^\diamond(x(t))), \varsigma_h^\diamond(x(t))) \equiv 0. \quad (12)$$

Differentiation of (12) w.r.t. x results in

$$\frac{d\psi_x}{dt} = - \left(\frac{\partial}{\partial x} f^t(x(t), \gamma_1^\diamond(x(t), \varsigma_h^\diamond(x(t))), \varsigma_h^\diamond(x(t))) \right)^\top \psi_x \quad (13)$$

which is evaluated along the semipermeable surfaces \mathcal{L} using

$$\dot{\psi}_x = \eta_x \quad (14)$$

at $t = \tau$ to ensure a smooth connection to the NUP. The computations resulting in (13) exploit the optimality of $\varsigma_h^\diamond(x(t))$ and $\gamma_1^\diamond(x(t), u_h(t))$ w.r.t. (11) (for details, see [15, p. 242]). By using the solution of (13) and (14), semipermeable surfaces \mathcal{L} that connect to the BNUP are constructed by solving

$$\dot{x}(t) = f^t(x(t), \gamma_1^\diamond(x(t), u_h(t)), \varsigma_h^\diamond(x(t))) \quad (15)$$

in retrograde time for all

$$x(\tau) \in \mathcal{S}, \quad (16)$$

which results in a set of trajectories

$$\xi(t; t_0, x(t_0), \gamma_1^\diamond(x, u_h), \varsigma_h^\diamond(x)), \text{ with } x(t_0) \in \mathcal{L}, \quad (17)$$

$$t_0 < \tau, \text{ and } \xi(\tau; t_0, x(t_0), \gamma_1^\diamond(x, u_h), \varsigma_h^\diamond(x)) \in \mathcal{S},$$

that can be parametrized by means of κ (see Remark 4).

If one or more semipermeable surfaces \mathcal{L} jointly subdivide Λ by intersecting with another \mathcal{L} or the NUP, a closed barrier \mathcal{K} is composed. If \mathcal{K} intersects itself, the portions beyond the intersection are to be discarded [16, Sec. 8.5].

B. Solving a Captivity-Escape Game of Kind with a Variable Planning Performance and Safety Bound

In contrast to Section V-A, consider both ϑ and α to be variable within this section. For addressing O.1, we aim to determine ϑ such that the semipermeable surfaces \mathcal{L} resulting from (15) and (16) jointly constitute a closed barrier \mathcal{K} that yields the captivity zone \mathcal{V}^- of a captivity-escape game of kind with $\beta = \alpha$ (see Theorem 1 and Corollary 2).

To highlight the dependency on ϑ and β , we denote the trajectories in (17) as $\xi_{\vartheta, \beta}^\mathcal{L}$. Moreover, we denote the part of $\xi_{\vartheta, \beta}^\mathcal{L}$ that contributes to constituting \mathcal{K} as $\xi_{\vartheta, \beta}^\mathcal{K}$: a part $\xi_{\vartheta, \beta}^\mathcal{K}$

starts in an intersection with another $\xi_{\vartheta,\beta}^{\mathcal{K}}$ or the NUP at $t = \hat{t}$ and ends when reaching the BNUP at $t = \tau$. Note that the initial time \hat{t} depends on the particular $x(\tau) \in \mathcal{S}$ related to the respective $\xi_{\vartheta,\beta}^{\mathcal{K}}$. Thus, the respective \hat{t} can be determined by means of a mapping $b(\kappa)$, $b: \mathbb{R}^r \rightarrow \mathbb{R}^{<\tau}$ (see Remark 4).

To potentially contain a part $\xi_{\vartheta,\beta}^{\mathcal{L}}$, trajectories $\xi_{\vartheta,\beta}^{\mathcal{L}}$ must approach the BNUP \mathcal{S} from the interior of Λ .

Proposition 2: Trajectories $\xi_{\vartheta,\beta}^{\mathcal{L}}$ approach the BNUP \mathcal{S} from the interior of the captivity set Λ , if

$$d^2/dt^2 \|c(\xi_{\vartheta,\beta}^{\mathcal{L}})\|_2|_{t=\tau} < 0. \quad (18)$$

Proof:

$$d/dt \|c(\xi_{\vartheta,\beta}^{\mathcal{L}})\|_2|_{t=\tau} = 0 \quad (19)$$

holds by Definition 21. If both (18) and (19) hold, τ is a strict local maximizer of $\|c(\xi_{\vartheta,\beta}^{\mathcal{L}})\|_2$ [18, Theorem 2.4]. The related maximum value is $\|c(\xi_{\vartheta,\beta}^{\mathcal{L}})\|_2|_{t=\tau} = \beta$ (see Remark 2). Thus, $\|c(\xi_{\vartheta,\beta}^{\mathcal{L}})\|_2 < \beta$ holds in a punctured neighborhood of τ , meaning that $\xi_{\vartheta,\beta}^{\mathcal{L}}$ approaches the BNUP \mathcal{S} from the interior of Λ , and also leaves \mathcal{S} into Λ . ■

Definition 24 requires $\xi_{\vartheta,\beta}^{\mathcal{K}} \subseteq \Lambda$ (see Definition 16).

Proposition 3: To ensure $\xi_{\vartheta,\beta}^{\mathcal{K}} \subseteq \Lambda$, the following must hold:

$$\|c(\xi_{\vartheta,\beta}^{\mathcal{K}})\|_2 \leq \beta, \quad \hat{t} \leq t \leq \tau. \quad (20)$$

Proof: Follows from Definition 11. ■

Moreover, to ensure \mathcal{V}^- is compact (see Assumption 5), trajectories $\xi_{\vartheta,\beta}^{\mathcal{L}}$ that contain a part $\xi_{\vartheta,\beta}^{\mathcal{K}}$ must not leave \mathcal{V}^- right after passing the BNUP \mathcal{S} .

Assumption 7: $\xi_{\vartheta,\beta}^{\mathcal{L}}$ contains a part $\xi_{\vartheta,\beta}^{\mathcal{K}}$.

Proposition 4: Let Assumption 7 be fulfilled. If

$$d/dt \xi_{\vartheta,\beta}^{\mathcal{L}}|_{t=\tau} \text{ points towards the NUP,} \quad (21)$$

and (18) holds, $\xi_{\vartheta,\beta}^{\mathcal{L}}$ leaves the BNUP \mathcal{S} into \mathcal{V}^- .

Proof: If Assumption 7 is fulfilled, \mathcal{S} separates the states on $\partial\Lambda$ leading to immediate escape from the states resulting in eternal captivity, i.e., the NUP (see Definition 10). ■

Corollary 5: Let Assumption 7 be fulfilled. For any $u_1 = \gamma_1(x, u_h)$, a trajectory $\xi(t; t_0, x(t_0), \gamma_1(x, u_h), \varsigma_h^{\diamond}(x))$ that solves (4) with $x(t_0) \in \mathcal{K}$ and $t_0 < \tau$, reaches the interior of \mathcal{V}^- at the latest after passing \mathcal{S} , if (18) is fulfilled.

Proof: The worst-case trajectory $\xi(t; t_0, x(t_0), \gamma_1^{\diamond}(x, u_h), \varsigma_h^{\diamond}(x))$ with $x(t_0) \in \mathcal{K}$ and $t_0 < \tau$ reaches the interior of \mathcal{V}^- after passing the BNUP \mathcal{S} at $t = \tau$ (see Proposition 4). Thus, any suboptimal $\gamma_1(x, u_h)$ results in a trajectory reaching the interior of \mathcal{V}^- sooner. ■

Corollary 6: If \mathcal{V}^- is nonempty, it is compact.

Proof: As Λ is compact (see Definition 11), the captivity zone $\mathcal{V}^- \subseteq \Lambda$ is bounded. Furthermore, the outlined method constructs $\partial\mathcal{V}^-$ utilizing the NUP and \mathcal{K} . If \mathcal{V}^- is nonempty, Corollary 5 ensures $\mathcal{K} \in \mathcal{V}^-$, and NUP $\subseteq \mathcal{V}^-$ results from Definition 20. Thus, \mathcal{V}^- is bounded and closed. ■

Depending on the employed planning and tracking models, (18), (20), and (21) can only be fulfilled for certain range of $\beta \geq \beta_{\min}$ and $\vartheta \leq \vartheta_{\max}$. The respective limits can be determined by solving (18), (20), and (21).

Consider the manifold, in which the parts $\xi_{\vartheta,\beta}^{\mathcal{K}}$ intersect with another $\xi_{\vartheta,\beta}^{\mathcal{K}}$ or the NUP for jointly composing a closed barrier \mathcal{K} , to be denoted as $\mathcal{M} \subseteq \Lambda$. For a given $\alpha = \beta \geq \beta_{\min}$, there can be various manifolds \mathcal{M} in which the parts $\xi_{\vartheta,\beta}^{\mathcal{K}}$

may intersect for jointly composing a closed barrier \mathcal{K} when fulfilling (18), (20), (21). Each of these manifolds \mathcal{M} relates to a different planning performance ϑ , and thus, there is a mapping $\nu(\vartheta, \beta)$, $\nu: \mathbb{R}^{+, \leq \vartheta_{\max}} \times \mathbb{R}^{\geq \beta_{\min}} \rightarrow \mathcal{P}(\mathcal{M})$.

Of particular interest is the mapping $\bar{\nu}(\beta)$, $\bar{\nu}: \mathbb{R}^{\geq \beta_{\min}} \rightarrow \mathcal{P}(\mathcal{M})$ that relates to the optimal ϑ to a given $\beta \geq \beta_{\min}$ via

$$\xi_{\vartheta,\beta}^{\mathcal{K}}|_{t=\hat{t}} \in \bar{\nu}(\beta). \quad (22)$$

For a specific pair of planning and tracking models, the mapping $\bar{\nu}(\beta)$ can be determined from offline optimizing ϑ subject to (18), (20), (21), and (22) for different $\beta \geq \beta_{\min}$.

Remark 5: If the tracking model is powerful enough to always remain within some distance from the planning model, \mathcal{V}^- exists [1], [2]. Thus, $\bar{\nu}(\beta)$ exists for a proper pair of planning and tracking models, if \mathcal{S} is nonempty and ϑ enables to sufficiently restrict \mathcal{X}_1 , \mathcal{U}_1 , and \mathcal{U}_1 (see Definition 5).

Remark 6: If desired, additional requirements can be considered by means of suitable objectives or constraints when determining $\bar{\nu}(\beta)$ (e.g., maximizing the extent of \mathcal{V}^- , etc.).

1) Addressing O.1 and O.0: Given $\alpha = \beta \geq \beta_{\min}$, O.1 is addressed by solving (18), (20), (21), and (22) for ϑ . Similarly, O.0 is addressed by solving the respective equations for $\alpha = \beta$, given $\vartheta \leq \vartheta_{\max}$ (or suitable \mathcal{X}_1 , \mathcal{U}_1 , and \mathcal{U}_1).

2) Addressing O.2 – The Safety Controller: To address O.2, the strategy $\varsigma_h^*(x)$ used in the minimal-intervention safety controller must be determined (see Theorem 3, Corollary 3).

Proposition 5: The optimal strategy $\varsigma_h^*(x)$ employed in Theorem 3 and Corollary 3 is given by

$$\varsigma_h^*(x) = \begin{cases} \varsigma_h^{\Delta}(x) & \text{if } x(t) \in \text{NUP} \subseteq \partial\mathcal{V}^-, \\ \varsigma_h^{\diamond}(x) & \text{if } x(t) \in \mathcal{K} \subseteq \partial\mathcal{V}^-. \end{cases} \quad (23)$$

Proof: The outlined method constructs $\partial\mathcal{V}^-$ utilizing the NUP and \mathcal{K} . For a state $x \in \text{NUP} \subseteq \partial\mathcal{V}^-$, the state-feedback strategy $u_h = \varsigma_h^{\Delta}(x)$ ensures $\eta_x^{\top} f^{\nu}(x(t), u_1(t), u_h(t)) \leq 0$ for any u_1 (see Definition 20). Similarly, for a state $x \in \mathcal{K} \subseteq \partial\mathcal{V}^-$, the strategy $u_h = \varsigma_h^{\diamond}(x)$ ensures to steer x into the interior of the captivity set \mathcal{V}^- (see Corollary 5). ■

VI. NUMERICAL EXAMPLE AND COMPARISON TO FASTRACK

In this section, we demonstrate our method and compare it to the state of the art. For notational brevity, we neglect dependencies on time and, e.g., write x instead of $x(t)$.

A. Setting up the Relative System

Consider the dynamics of the widely-used homicidal chauffeur game formulated in [16, Example 2.1.2]. The low-fidelity planning model employs the dynamics of the pedestrian, and the high-fidelity tracking model employs the dynamics of the chauffeur. The state vectors are given by $x_1 = [x_1 \ y_1]^{\top}$ and $x_h = [x_h \ y_h \ \varphi_h]^{\top}$, and the dynamics are given by

$$\dot{x}_1 = \begin{bmatrix} v_1 \sin(u_1) \\ v_1 \cos(u_1) \end{bmatrix} \text{ and } \dot{x}_h = \begin{bmatrix} v_h \sin(\varphi_h) \\ v_h \cos(\varphi_h) \\ \omega_h u_h \end{bmatrix}, \quad (24)$$

with the inputs $|u_h| \leq 1$ and $|u_1| \leq \pi$, constant velocities $0 \leq v_1 < v_h$, and the tracking model's maximum yaw rate

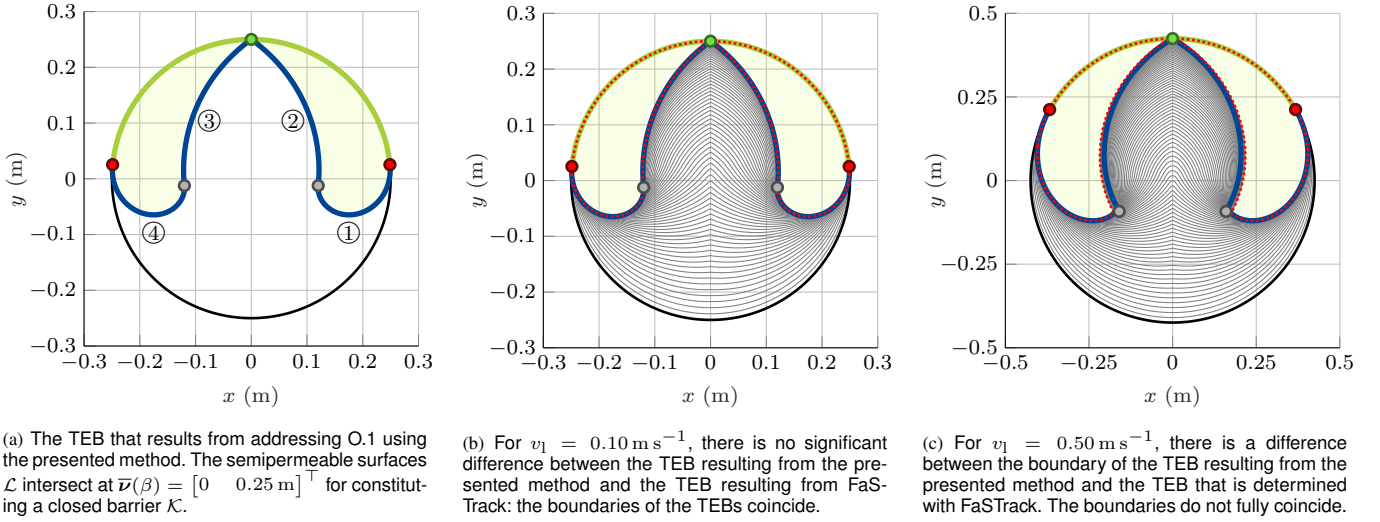


Fig. 3 The TEB resulting from the presented method is depicted by the green area. The black circle depicts the boundary of the captivity set $\partial\Lambda$, the green line depicts the NUP, and the blue line depicts the closed barrier \mathcal{K} . The red dots depict the BNUP, the green dots depict $\bar{\mathbf{p}}(\beta)$, and the gray dots depict where u_h^\diamond switches (see (30b)). The gray lines illustrate how the numerical FaSTrack computations evolve, starting in $\partial\Lambda$ and converging to the dotted red line, which depicts the boundary of the TEB determined with the method in FaSTrack.

$0 \leq \omega_h < \infty$. Thus, \mathbf{u}_1 only contains one parameter: $u_1 = v_1$. As constraining the planning model per se in x_1, y_1 , or u_1 is impractical for motion planning, we use $\vartheta = \theta = v_1$.

The state vector of the related relative system is given by

$$\mathbf{x} = \begin{bmatrix} x \\ y \\ \varphi_h \end{bmatrix} = \Phi(\mathbf{x}_1, \mathbf{x}_h) \left(\mathbf{Q} \begin{bmatrix} x_1 \\ y_1 \end{bmatrix} - \begin{bmatrix} x_h \\ y_h \\ \varphi_h \end{bmatrix} \right), \quad (25)$$

which is aligned to the orientation of the tracking model using

$$\Phi(\mathbf{x}_1, \mathbf{x}_h) = \begin{bmatrix} \cos(\varphi_h) & -\sin(\varphi_h) & 0 \\ \sin(\varphi_h) & \cos(\varphi_h) & 0 \\ 0 & 0 & -1 \end{bmatrix} \text{ and } \mathbf{Q} = \begin{bmatrix} 1 & 0 \\ 0 & 1 \\ 0 & 0 \end{bmatrix}. \quad (26)$$

As the planning model fully controls the relative orientation ($\varphi_h - u_1$), the state φ_h becomes obsolete; thus, $\mathbf{x} = [x \ y]^T$. The relative dynamics $\mathbf{f}^r(\mathbf{x}(t), u_1(t), u_h(t))$ are given by

$$\begin{bmatrix} \dot{x} \\ \dot{y} \end{bmatrix} = \begin{bmatrix} -y\omega_h u_h + v_1 \sin(u_1) \\ x\omega_h u_h + v_1 \cos(u_1) - v_h \end{bmatrix}. \quad (27)$$

B. Solving the Related Game with Variable ϑ and β

To consider safety-critical constraints in the x - y -plane, $\mathbf{c}(\mathbf{x}) = \mathbf{x}$ is required, which yields $\boldsymbol{\eta}_x = \mathbf{x}$, $\mathbf{x} \in \partial\Lambda$. Solving (10) yields the NUP $\{\mathbf{x} \in \partial\Lambda \mid \beta v_1/v_h \leq y\}$ and the BNUP

$$\mathcal{S} = \left\{ \mathbf{x} \in \partial\Lambda \mid x = \beta \sqrt{1 - (v_1/v_h)^2}, y = \beta v_1/v_h \right\}, \quad (28)$$

containing two states that are symmetrical about the y -axis. Thus, there are two $\xi_{\vartheta, \beta}^{\mathcal{L}}$, each constituting one semipermeable surface \mathcal{L} . For determining the optimal $u_h^\diamond = \varsigma_h^\diamond(\mathbf{x})$ and $u_1^\diamond = \gamma_1^\diamond(\mathbf{x}, u_h)$ that define \mathcal{L} , (27) is inserted into (11):

$$\min_{u_h \in \mathcal{U}_h} \max_{u_1 \in \mathcal{U}_1} (\psi_x(-y\omega_h u_h + v_1 \sin(u_1)) + \psi_y(x\omega_h u_h + v_1 \cos(u_1) - v_h)) = 0. \quad (29)$$

Solving (29) for u_h and u_1 yields

$$u_1^\diamond = \arcsin(\psi_x / \|\psi_x\|_2) = \arccos(\psi_y / \|\psi_x\|_2), \quad (30a)$$

$$u_h^\diamond = \text{sgn}(\psi_x y - \psi_y x), \quad (30b)$$

which is used for determining the evolution of ψ_x using (13):

$$\dot{\psi}_x = [-\psi_y \omega_h u_h^\diamond \ \psi_x \omega_h u_h^\diamond]^T. \quad (31)$$

Solving (31) results in

$$\psi_x = \begin{bmatrix} \psi_x \\ \psi_y \end{bmatrix} = \begin{bmatrix} \rho \cos(\omega_h u_h^\diamond \cdot (t - \tau) + \delta) \\ \rho \sin(\omega_h u_h^\diamond \cdot (t - \tau) + \delta) \end{bmatrix}. \quad (32)$$

At $t = \tau$, (14) must hold. Equation (28) and $\boldsymbol{\eta}_x = \mathbf{x}$ yield

$$\delta = \arcsin\left(\frac{\beta v_1}{\rho v_h}\right) = \arccos(\beta \sqrt{1 - (v_1/v_h)^2}/\rho). \quad (33)$$

As only the direction of ψ_x is relevant, β/ρ is neglected in (33). The trajectories $\xi_{\vartheta, \beta}^{\mathcal{L}}$ result from solving

$$\begin{bmatrix} \dot{x} \\ \dot{y} \end{bmatrix} = \begin{bmatrix} -y\omega_h u_h^\diamond + v_1 \cos(\omega_h u_h^\diamond \cdot (t - \tau) + \delta) \\ x\omega_h u_h^\diamond + v_1 \sin(\omega_h u_h^\diamond \cdot (t - \tau) + \delta) - v_h \end{bmatrix} \quad (34)$$

for both states in (28) that must hold at $t = \tau$ (see (15), (16)). The two resulting $\xi_{\vartheta, \beta}^{\mathcal{L}}$ are symmetrical about the y -axis.

For better comparison to FaSTrack, we require $\bar{\mathbf{p}}(\beta) = [0 \ y_0]^T$, $|y_0| \leq \beta$ so that the resulting TEB is connected. Optimizing ϑ w.r.t. (18), (20), (21) yields $\bar{\mathbf{p}}(\beta) = [0 \ \beta]^T$. So

$$\xi_{\vartheta, \beta}^{\mathcal{L}}|_{t=\hat{t}} = [0 \ \beta]^T \quad (35)$$

must hold for both $\xi_{\vartheta, \beta}^{\mathcal{L}}$.

C. Addressing O.0, O.1, and O.2 Using the Game

In the sequel, we use $v_h = 1 \text{ m s}^{-1}$ and $\omega_h = 2\pi \text{ rad s}^{-1}$.

1) **Addressing O.1:** Consider the safety margin to be given with $\alpha = 0.25 \text{ m}$. Solving (35) with $\beta = \alpha$ results in $v_1 \approx 0.10 \text{ m s}^{-1}$.⁶ The resulting TEB \mathcal{B} is depicted in Fig. 3a.

2) **Addressing O.2:** The safety controller results from (30b):

$$\bar{\varsigma}(\mathbf{x}) = \begin{cases} 1 & \text{if } \mathbf{x} \in \partial\mathcal{B} \text{ at } \textcircled{1} \text{ or } \textcircled{3}, \\ -1 & \text{if } \mathbf{x} \in \partial\mathcal{B} \text{ at } \textcircled{2} \text{ or } \textcircled{4}, \\ \text{any } u_h \in [-1, 1] & \text{if } \mathbf{x} \in \text{int}(\mathcal{B}) \cap \text{NUP} \setminus \mathcal{S}. \end{cases} \quad (36)$$

⁶Wolfram Mathematica determines an accurate but lengthy solution.

3) *Addressing O.0*: Consider the inverse task of the task solved in Section VI-C.1, with $v_1 = 0.10 \text{ m s}^{-1}$ given. Solving (35) with $\vartheta = v_1$ results in $\alpha = \beta \approx 0.25 \text{ m}$.⁶

D. Comparison to FaSTrack

For comparing our method to the state of the art, O.0, as formulated in Section VI-C.3, is addressed with the method in FaSTrack for both $v_1 = 0.10 \text{ m s}^{-1}$ and $v_1 = 0.50 \text{ m s}^{-1}$. To this end, we use the helperOC⁷ toolbox and discretize the state space with $\Delta x = \Delta y = 1 \times 10^{-3} \text{ m}$ and $\Delta \varphi = 8.73 \times 10^{-3} \text{ rad}$.⁸ The resulting TEBs for $v_1 = 0.10 \text{ m s}^{-1}$ and $v_1 = 0.50 \text{ m s}^{-1}$ are depicted in Fig. 3b and Fig. 3c, respectively.

E. Discussion

As demonstrated in Section VI-C, the presented method addresses O.0, O.1, and O.2. All presented results are determined using Wolfram Mathematica to ensure numerical accuracy.

For addressing O.0, there is no significant difference between the TEB determined with the presented method and the TEB determined with FaSTrack for $v_1 = 0.10 \text{ m s}^{-1}$ (see Fig. 3b). This demonstrates that, aside from numerical discrepancies, our method yields the same TEB as the method in FaSTrack, which is the least conservative method for addressing O.0 in the literature. However, for $v_1 = 0.50 \text{ m s}^{-1}$, there is a difference in the TEB determined with our method and the TEB determined with the method in FaSTrack (see Fig. 3c). This indicates the effects of the numerical methods involved in FaSTrack, even at the stated accuracy.⁹

All presented results are computed on an Intel® Core™ i9-12900 processor with 128 GB RAM. The CPU time for determining the TEB with FaSTrack at the stated accuracy is $3.13 \times 10^5 \text{ s}$ for $v_1 = 0.10 \text{ m s}^{-1}$ and $1.15 \times 10^6 \text{ s}$ for $v_1 = 0.50 \text{ m s}^{-1}$. The CPU time for addressing O.0 with our method is 18.17 s (see Section VI-C.3), independently of the value of v_1 . The CPU time for addressing O.1 with our method is 1.79 s (see Section VI-C.1), and the optimization for determining $\bar{\nu}(\beta)$ took less than 1 s. The computation time of our method can be reduced to less than 10 ms by solving (22) numerically using a C++ implementation.¹⁰ This enables online adaption of the planning performance to a given safety margin for reducing conservatism in safe motion generation.

VII. CONCLUSION

In this paper, we have presented a method that addresses the conservatism, computational effort, and limited numerical accuracy of existing frameworks and methods that ensure safety in online model-based motion generation. In contrast to existing approaches that determine a safety margin based on a given pair of models, we adopt a different perspective and directly adapt the performance of the planning model to

a given safety margin. This change in perspective enables the mitigation of conservatism in existing frameworks that ensure safety in motion generation. By leveraging a captivity-escape game, a specific zero-sum differential game formulated in this paper, our method requires significantly less computation time compared to the state of the art, and in contrast to the state-of-the-art method, our method yields numerically accurate results. With these benefits, our method complements established frameworks, making them even more effective.

REFERENCES

- [1] S. L. Herbert *et al.*, “Fastrack: A modular framework for fast and guaranteed safe motion planning,” in *2017 IEEE 56th Conf. Decis. Control*, 2017, pp. 1517–1522.
- [2] M. Chen *et al.*, “Fastrack: A modular framework for real-time motion planning and guaranteed safe tracking,” *IEEE Trans. Autom. Control*, vol. 66, no. 12, pp. 5861–5876, 2021.
- [3] S. Singh, M. Chen, S. L. Herbert, C. J. Tomlin, and M. Pavone, “Robust tracking with model mismatch for fast and safe planning: An sos optimization approach,” in *Algorithmic Foundations Robot. XIII*, Springer, 2020, pp. 545–564.
- [4] S. Kousik, S. Vaskov, F. Bu, M. Johnson-R., and R. Vasudevan, “Bridging the gap between safety and real-time performance in receding-horizon trajectory design for mobile robots,” *Int. J. Robot. Res.*, vol. 39, no. 12, pp. 1419–1469, 2020.
- [5] *Road vehicles — Functional safety*, ISO 26262, 2018.
- [6] B. Schürmann, M. Klischat, N. Kochdumper, and M. Althoff, “Formal safety net control using backward reachability analysis,” *IEEE Trans. Autom. Control*, vol. 67, no. 11, pp. 5698–5713, 2022.
- [7] J. F. Fisac *et al.*, “A general safety framework for learning-based control in uncertain robotic systems,” *IEEE Trans. Autom. Control*, vol. 64, no. 7, pp. 2737–2752, 2019.
- [8] I. Mitchell, A. Bayen, and C. Tomlin, “A time-dependent hamilton-jacobi formulation of reachable sets for continuous dynamic games,” *IEEE Trans. Autom. Control*, vol. 50, no. 7, pp. 947–957, 2005.
- [9] E. A. Coddington and N. Levinson, *Theory of Ordinary Differential Equations*. Melbourne, FL, USA: Krieger, 1984.
- [10] J. Köhler, R. Soloperto, M. A. Müller, and F. Allgöwer, “A Computationally Efficient Robust Model Predictive Control Framework for Uncertain Nonlinear Systems,” *IEEE Trans. Autom. Control*, vol. 66, no. 2, pp. 794–801, 2021.
- [11] D. Fridovich-Keil, S. L. Herbert, J. F. Fisac, S. Deglurkar, and C. J. Tomlin, “Planning, fast and slow: A framework for adaptive real-time safe trajectory planning,” in *2018 IEEE Int. Conf. Robot. Automat.*, 2018, pp. 387–394.
- [12] A. Sahraeeekhanghah and M. Chen, “Pa-fastrack: Planner-aware real-time guaranteed safe planning,” in *2021 60th IEEE Conf. Decis. Control*, 2021, pp. 2129–2136.
- [13] A. Quarteroni, R. Sacco, and F. Saleri, *Numerical Mathematics*. Berlin Heidelberg: Springer, 2010.
- [14] L. C. Evans and P. E. Souganidis, “Differential games and representation formulas for hamilton-jacobi-isaacs equations,” *Indiana Univ. Math. J.*, vol. 33, no. 5, pp. 773–797, 1984.
- [15] T. Basar and G. J. Olsder, *Dynamic Noncooperative Game Theory*. Philadelphia, PA, USA: SIAM, 1999.
- [16] R. Isaacs, *Differential Games: A Mathematical Theory with Applications to Warfare and Pursuit, Control and Optimization*, New ed Edition. Dover Publications Inc., 1999.
- [17] J. Lewin, *Differential Games*. London, UK: Springer, 1994.
- [18] J. Nocedal and S. J. Wright, *Numerical Optimization* (Springer Series in Operations Research and Financial Engineering). New York, NY, USA: Springer, 2006.
- [19] I. M. Mitchell, “Application of level set methods to control and reachability problems in continuous and hybrid system,” Ph.D. dissertation, Stanford Univ., 2002.

⁷<https://www.github.com/HJReachability/helperOC>

⁸Using (25) results in numerical oscillations that degenerate the solution. Therefore, $\tilde{x} = Qx_1 - x_h$ is used, for which FaSTrack yields a stable solution.

⁹The discrepancy is hypothetically rooted in the kink in \mathcal{K} (at the states in which v_h^* switches), which causes dissipation as described in [19, Sec. 2.2.1].

¹⁰Note that it can still be checked if the numerical accuracy of the result ensures safety by inserting the result into (22).